This is the pre-peer reviewed version of the following article: **[J. Reolid; C. Betzler; J.C. Braga; T. Lüdmann; A. Ling; G.P. Eberli. Facies and geometry of drowning steps in a Miocene carbonate platform (Maldives). Palaeogeography, Palaeoclimatology, Palaeoecology. 538, pp. 109455. 2020],** which has been published in final form at **[https://doi.org/10.1016/j.palaeo.2019.109455].** This article may be used for non-commercial purposes in accordance with Elsevier Terms and Conditions for Use of Self-Archived Versions

Abstract

The study of the Miocene carbonate platform of the Maldives allows understanding the controlling factors triggering the stepwise drowning of carbonate platforms. This research presents high-resolution seismic profiles and sediment cores retrieved from Sites U1465, U1469, and U1470 drilled during International Ocean Discovery Program (IODP) Expedition 359. A microfacies analysis of the platform deposits was conducted and correlated with a sequence stratigraphic analysis of seismic reflection data. The Neogene evolution of the Maldives encompasses a series of drowning steps. Two of these steps are compared with regard to the carbonate factory type to unravel if fossil assemblage surviving the first drowning step are different from younger assemblages. In both cases the shallow water carbonate facies are formed by coral-coralline algal boundstone and foralgal floatstone that change basinwards into slope facies dominated by large benthic foraminifera grainstone to packstone, locally floatstone and rudstone. The red algae and large benthic foraminifera assemblages are similar before and after the first drowning step. After this first drowning, the carbonate platform developed under enhanced bottom current conditions, as deduced by the coeval drift deposits. The carbonate platform and the drift deposits were balanced for circa 2 Myr, until a global sea-level fall at 10.6 Ma

and later reflooding of the platform, which destroyed the equilibrium between both depositional systems, favouring the current-controlled deposits. The drowning of the Miocene carbonate platform of the Maldives was the result of the combined effect of the fluctuating sea-level during the Neogene and the intensification of oceanic currents due to the invigoration of the South Asian Monsoon during the middle Miocene.

Keywords: carbonate facies; coral reef; sea level; oceanic currents; Leg 359; eustasy.

1. Introduction

The study of the drowning history of carbonate platforms in recent years focused on determining the environmental reconstruction leading to drowning events (Erlich et al., 1990; Weissert et al., 1998; Betzler et al., 2009; Sattler et al., 2009; Eberli et al., 2010). Drowning of a shallow-water carbonate platform occurs when the rate of increasing accommodation space exceeds the rate of carbonate accumulation or when the growth rates are reduced by environmental disturbance (Schlager, 1981). Anoxic events, tectonic breakup, nutrient excess, increased rates of subsidence, or action of strong currents have been invoked to explain this process (Arthur and Schlager, 1979; Schlager, 1981, 1989; Hallock and Schlager, 1986; Schlager and Camber, 1986; Erlich et al., 1990; Eberli, 1991; Weissert et al., 1998; Betzler et al., 2009; Sattler et al., 2009; Eberli et al., 2010). The sedimentary sequence produced during drowning is known as a drowning sequence (Erlich et al., 1990). Understanding these sequences does not only provide information about palaeoenvironmental perturbations but has also an applied focus because many hydrocarbon reservoirs are related to fossil carbonate platforms capped by drowning sequences and unconformities (Wilson and Hall, 2010; Burchette, 2012).

The Maldives carbonate edifice recorded a series of drowning steps from the middle Miocene to Pliocene (Betzler et al., 2009, 2013, 2016, 2017, 2018; Lüdmann et al., 2013).

The drowning process was studied by Betzler et al. (2009, 2013) and by Lüdmann et al. (2013), and interpreted as a result of bottom current intensification and increased nutrient supply. It is widely accepted that of nutrient excess cause the demise of carbonate platforms by the growth of plankton that reduces water transparency and accordingly the carbonate production by zooxanthellate corals and calcareous algae (Hallock and Schlager, 1986). In the area of the Kardiva Channel, especially to the north of Goidhoo atoll at the position of IODP Sites U1465 and U1469 (Fig. 1) the drowning of the Miocene platform occurred at 13 Ma and is marked by the distinctive sequence boundary DS1 (Betzler et al., 2013, 2016, 2017; Lüdmann et al., 2013). In contrast, in the southern branch of the western Kardiva Channel, at the location of IODP Site U1470, shallow-water carbonate production above DS1 (Betzler et al., 2017) persisted for circa 2 Myr.

This study aims to develop a stratigraphy of the drowned platform parts in the northern and southern branches of the western Kardiva Channel in order to understand the Miocene drowning of the Maldives. To achieve this goal, a microfacies analysis of the platform deposits was conducted and correlated with sequence stratigraphic analysis of seismic reflection data. The data for this study were retrieved from Sites U1465, U1469, and U1470 drilled during International Ocean Discovery Program (IODP) Expedition 359 (2015), and high-resolution seismic data from scientific cruises NEOMA (2007) and SO236 (2014).

The study of the drowning will improve the knowledge about the reasons why carbonate systems, particularly reefs, drowned in the past, and might help in understanding the factors that control the demise of modern reefs (Sattler et al., 2009).

2. Geological setting

The Maldives archipelago is an isolated carbonate platform in the central-equatorial Indian Ocean located to the southwest of India and Sri Lanka (Fig. 1). A double row of atolls encloses the up to 500 m deep Inner Sea basin which is connected to the open Indian Ocean by inter-atoll channels. Atolls initiated as relict banks through a series of middle Miocene to Pliocene drowning steps (Betzler et al., 2009, 2013, 2016, 2017, 2018; Lüdmann et al., 2013). Current-controlled deposits overlie drowned banks and their basinward-facing flanks (Lüdmann et al., 2013). Such deposits represent the latest stage of a dynamic geological evolution of a 3-km thick carbonate edifice from the Palaeocene to the present (Duncan and Hargraves, 1990; Aubert and Droxler, 1992; Purdy and Bertram, 1993; Belopolsky and Droxler, 2003; Betzler et al., 2013).

The study focuses on the elevated platform rims that since the early Miocene produced an inner basin occupying the platform interior. During the late middle Miocene, some banks continued prograding, while others partially drowned and were overlain by drift deposits (Lüdmann et al., 2013; Belopolsky and Droxler 2003, 2004a, b; Betzler et al., 2013, 2017; Reolid et al., 2017a; 2019). The drift deposits consist of hemipelagic sediments and reworked periplatform ooze. The transition from a sea-level to a current-controlled system was attributed to the intensification of the Indian Monsoon (Betzler et al., 2009, 2013, 2016, 2017, 2018; Lüdmann et al., 2013).

3. Methods

During IODP Expedition 359, Sites U1465 (4°55.9873’N, 073°0.6786’E), U1469 (4°54.4143’N, 073°0.4910’E), and U1470 (4°45.9828’N, 072°59.0324’E) were cored in the Inner Sea to recover a sedimentary sequence encompassing the Miocene platform carbonates of the Maldives (Fig. 1). Core retrieval, handling and all on board measurements on the cores as well as the downhole logging are described in detail in Betzler et al. (2017). For Site U1465 three holes were drilled while two holes were drilled for Site U1470. The stratigraphic columns presented in Figures 2 and 3 integrate the information of every hole at each site. The values of the natural gamma radiation were obtained by the Natural Gamma Radiation Logger (NGR) (Betzler et al., 2017). The different facies and sedimentary features were based on visual core description backed up by the analysis of 164 thin-sections. The carbonates were classified according to Dunham (1962) and Embry and Klovan (1972). The relative abundance of the bioclastic components follows the terminology of Betzler et al. (2017): abundant (>20% of field of view), common (>5%–20% of field of view), few (1%–5% of field of view), rare (<1% of field of view), and present (1 per 10 fields of view). The age assignments of the successions drilled rely on calcareous nannoplankton and planktonic foraminifer events (Betzler et al., 2016, 2017, 2018).

Prior to the drilling of Sites U1465, U1469, and U1470, a sequence stratigraphic analysis was performed based on seismic data (Betzler et al., 2013; Lüdmann et al., 2013). The seismic stratigraphy of the Miocene carbonate platform at the western Kardiva Channel (WKC) focuses on five seismic lines (Fig.1). Four lines, P65, P32, P47, and P62 are oriented west-east whereas the fifth one, P44, is a crossing line, in north-south direction (Fig. 1). Erosional truncations and onlap geometries were applied to define sequence boundaries according to the terminology proposed by Mitchum et al. (1977). Eleven sequences for the platform succession were differentiated, labelled ps1-ps11 and their lower boundaries PS1-PS11, and ten drift sequences labelled ds1-ds10. The core to seismic correlation relies on fixed points provided by the cores, such as the contacts between consolidated and unconsolidated materials or sudden changes in fossil assemblages.

4. Results

4.1 Sedimentary succession

The facies succession of the Miocene carbonate platform of the Maldives is different from the northernmost Sites U1465 and U1469 (Fig. 2) to Site U1470 (Fig. 4) in the southern branch of the WKC (Fig. 1). The facies of the platform succession are described in detail in Table 1.

4.1.1 Northern branch of the western Kardiva Channel

Site U1465 penetrated a series of clinoforms erosively capped by DS1 (Fig. 2). Clinoform deposits are attributed to ps10 and ps11 (Betzler et al., 2017). The facies in the interval from 233.2 mbsf, the bottom of the Site, to 162.9 mbsf consists of a larger benthic foraminifera grainstone (LBF grainstone, Fig. 2). *Halimeda* is common to abundant and homogeneously distributed throughout the succession. Among the large benthic foraminifera, *Amphistegina* is common throughout, while *Operculina* varies between rare and few. The amount of *Miogypsina* decreases up core until it finally disappears at the top of this interval. Other LBF and small benthic foraminifera, as well as coral debris are relatively rare to absent at the bottom, and gradually become more significant up core. The occurrence of coralline red algae varies from present to common. Among the coralline algae there are abundant fragments of *Adeylithon* (= *Aethesolithon* Johnson; Peña et al., 2018), common melobesiods (mainly *Lithothamnion*) and *Sporolithon*, as well as *Lithophyllum*, *Harveylithon*, *Lithoporella*, *Porolithon*, *Neogonilithon*, and *Hydrolithon* in different amounts. Between 220 and 200 mbsf there is an interval of coarse-grained grainstone, grainstone-rudstone. Except for this interval the succession is characterised by an alternation of poorly-cemented and well-cemented grainstone (Fig. 5a). When recovery allows to observe facies changes, the alternation mostly shows gradual transitions, although sharp contacts were also observed.

At 162.9 mbsf there is the base of an interval of a LBF packstone to grainstone with abundant LBF and calcareous-algal fragments (Fig. 5b). This interval extends up to 105 mbsf, with two intercalations of other facies. From 153 to 143 mbsf there is a LBF rudstone with abundant benthic foraminifera and few calcareous algae, delimited by a sharp contact at the base (Fig. 6a). Among the algae, in this facies there are *Halimeda* and coralline algae including fragmented *Adeylithon*, *Neogoniolithon* and other unidentifiable genera. About a half of the LBF are large, thick, rounded *Amphistegina*. *Operculina* fragments are common, and individuals are up to 7 mm in size with mostly scarce fragmentation. Several thin and large *Cycloclypeus* (0.5 and 4 mm respectively) were observed. *Lepidocyclina* is present with specimens up to 5 mm in diametre.

At ~133 mbsf there is the base of an interval of floatstone to packstone rich in LBF and other large bioclasts (Fig. 6b). Coralline algae are represented by variable amounts of *Neogoniolithon*, *Lithothamnion*, *Harveylithon*, and *Adeylithon*.

A foralgal floatstone occurs from 105 to 66 mbsf with an intercalation of rhodalgal rudstone (Fig. 2). Corals, encrusting foraminifera, bryozoans, planktonic foraminifera, and few LBF appear in this interval (Fig. 7a). The coralline algae assemblage is dominated by *Neogoniolithon* and *Adeylithon*, with minor *Lithophyllum*, *Harveylithon*, *Hydrolithon*, *Mesophyllum*, and unidentifiable melobesiod. The intercalated rhodalgal rudstone at 90 mbsf is poor in LBF and rich in *Adeylithon*, and *Halimeda* (Fig. 6c). The facies changes gradually from floatstone to rudstone at 75 mbsf. Planktonic foraminifera are present to absent in the upper part of the interval. The uppermost part of this interval shows geopetal structures with micrite infill (Fig. 8). Small planktonic foraminifera floating in the micritic matrix may occur. Locally, the top of the platform succession consists of a few-centimetre-thin interval of coral-coralline algal boundstone (Fig. 2). The top of the platform is partially eroded at Site U1465 (Lüdmann et al., 2013), but it is preserved at Site U1469 (Fig. 3). The sediments at this site consists of an intensely dolomitised foralgal floatstone with common to few coralline algae (*Adeylithon* and *Mesophyllum*), mollusks, and *Amphistegina*. Coral debris and some *Operculina* may be present (Fig. 3). The contact between the platform and the overlying grainstone to rudstone from the drift deposits was not recovered.

4.1.2 Southern branch of the western Kardiva Channel

The cores recovered at Site U1470 encompass a shallow-water succession of sequences ps9 to ds2. The succession at this site starts with an interval of coral-coralline algal boundstone from 343.7 to ~334 mbsf (Fig. 2). Benthic and planktonic foraminifera are also present. From ~334 to 324 mbsf there is a ~10 m thick package of foralgal floatstone to rudstone rich in red algae and *Amphistegina*. *Halimeda*, encrusting foraminifera, bryozoans, and small benthic foraminifera are rare to few while LBF, including *Lepidocyclina*, *Operculina*, *Borelis*, *Marginopora*, and *Sorites,* are present (Fig. 2). Among the red algae there are fragments of *Adeylithon*, *Neogoniolithon*, *Lithophyllum*, and *Lithoporella*.

From ~322 to 315 mbsf, above PS10 the LBF there is a packstone to grainstone overlain by a ~10 m thick intercalation of coral-coralline algal boundstone (Figs. 2 and 5). The packstone to grainstone has rare to few coralline algae, *Halimeda*, miliolids and other small benthic foraminifera, *Amphistegina*, and *Sorites*, while planktonic foraminifera, *Miogypsina*, and *Marginopora* are only present. The coral-coralline algal boundstone is similar to that at the base of the succession but with a higher proportion of red algae, mostly *Adeylithon* and minor *Neogoniolithon*.

The top of the coralgal boundstone corresponds to PS11. Above the sequence boundary the succession consists of a LBF packstone to grainstone which at 275 mbsf is overlain by a mixed benthic foraminifera floatstone (Fig. 9). *Marginopora*, *Amphistegina*, miliolids, and other small benthic foraminifera are rare to few. Red algae, *Halimeda*, encrusting foraminifera and bryozoans, *Operculina*, and *Sorites* are present. A mixed benthic foraminifera packstone occurs from 268 to 227 mbsf (Fig. 2). This facies is rich in LBF and locally presents intraclasts.

At 227 mbsf, at DS1 there is the base of a 20 m-thick interval of foralgal floatstone to rudstone (Fig. 2). Mollusks are common throughout the interval, especially oyster fragments (Fig. 7b). Above this facies, at ~207 mbsf, there is a grainstone rich in large benthic foraminifera. Coralline algae, *Halimeda*, encrusting foraminifera, bryozoans, planktonic and small benthic foraminifera are present in variable amounts throughout the 10-m-thick interval (Figs. 2 and 5). Fragments of *Adeylithon*, *Sporolithon*, *Lithothamnion*, and *Neogoniolithon* are the most representative red algae. Miliolids, *Borelis*, *Marginopora*, and intraclasts are present above ~200 mbsf. Echinoids spines and plates are common to abundant in this facies (Fig. 2).

The amount of corals and coralline algae increases upcore in a foralgal floatstone extending from 198 to ~179 mbsf, whereas the proportion of miliolids and LBF decreases (Figs. 2 and 7). The red algal assemblage includes *Adeylithon*, *Neogoniolithon*, *Hydrolithon*, and *Lithophyllum*. From ~178 to 167 mbsf there is an interval of coral-coralline algal boundstone especially rich in red algae with a small amount of *Halimeda*, encrusting foraminifera, and bryozoans. The red algal assemblage is dominated by *Neogoniolithon* and *Hydrolithon*, with secondary *Lithophyllum* and *Adeylithon*. Planktonic foraminifera are also more abundant here than in the other intervals with similar facies. The coral-coralline algal boundstone is overlain by an interval of foralgal floatstone. The platform succession at this site ends with another interval of coral-coralline algal boundstone, 10 m in thickness, topped by a thin interval of foralgal floatstone with some intraclasts (Fig. 2). The foralgal floatstone is dominated by *Adeylithon* in contrast with the abundant *Neogoniolithon* of the boundstone. The platform facies above DS3 are overlain by a planktonic foraminifera-rich grainstone typical of the drift deposits (Betzler et al., 2017).

4.2 Core-to-seismic correlation

4.2.1 Northern branch of western Kardiva Channel

Line P65 is W-E oriented and crosscut the northern branch of the WKC at the position of Site U1465 (Fig. 1). The profile shows clinoformal prograding geometries of the platform sequences with oblique-tangential pattern and toplap terminations (Fig. 9). The internal configuration of ps10 exhibits basinward dipping, medium-amplitude reflections (Fig. 10). The succession from the bottom of the hole to 163 mbsf including a LBF grainstone is the core equivalent of subparallel-oblique reflections that onlap and downlap the sequence boundary PS10 (Fig. 10). The reflections comprised in this wedge have more amplitude and are more continuous towards the slope. From 163 to 138 mbsf, the rudstone to packstone rich in LBF belongs to the upper part of the platform sequence ps10. The seismic geometries equivalent to the LBF packstone to rudstone consist of chaotic reflections to the top of the sequence, which change basinward into discontinuous sigmoidal reflections of medium amplitude towards basin interior. The LBF grainstone correlates well to a body with onlapping and downlapping reflections that can be interpreted as a lowstand wedge (Figs. 2 and 10). The overlying reflections corresponding to the LBF packstone may therefore be interpreted as the transgressive package.

The deposits between 138 mbsf and 66 mbsf are included in sequence ps11 (Fig. 10), which is marked by moderately continuous, sub-horizontal to gently dipping reflections at the location of U1465. The proximal parts of ps11 have chaotic reflections. Further downslope, the dipping foresets exhibit almost vertical reflections of low-amplitudes. The bottomsets, similarly to the underlying sequences, consist of continuous high-amplitude reflections. No clear terminations were identified throughout this sequence. The boundary DS1 defines the top of the platform deposits. On the flat platform top, around 700 ms TWT, drift sequences DS2– DS6 converge (Fig. 10). The top of platform sequences ps10 and ps11 are not preserved in line P65 because of erosional unconformity formed by channel incision and removal of the topsets in the center of the northern Kardiva Channel during partial platform drowning (Lüdmann et al., 2013, 2018).

Line P32, situated 2.9 km south from line P65 (Fig. 1), contains Site U1469 and shows the complete platform succession without the channel erosion of the platform top (Fig. 11). Line P32 displays clinoformal prograding geometries of the platform sequences with aggradation of the topsets. The preserved top of ps11 in this area imaged reflections with toplap termination (Fig. 11).

4.2.2 Southern branch of western Kardiva Channel

South of Goidhoo Atoll, line P47 shows large areas with chaotic seismic reflection pattern, likely because of fluid flow or sand injection that makes the tracing of sequence boundaries very difficult (Fig. 11). However, sequences ps8 to ps11 apparently show sigmoid-oblique aggradational to progradational clinoforms. The platform top in P47, around 750 ms, presents high-amplitude reflections that are truncated at the sequence boundary DS1. The platform slope appears to be gentler than in the north, and includes some contorted high-amplitude reflections at its upper part covering wavy, chaotic reflections. Both parallel lines P47 and P62, 1.7 km south from line P47, show a chaotic internal reflection pattern at the slope (Figs. 10 and 12) because of the up flow of fluid or unconsolidated materials. These injections penetrates the layering of the platform sequences and uplifts the uppermost strata including DS1, D2 and DS3.

Line P62 crosscuts the southern branch of the WKC at the position of Site U1470 (Fig. 1). From PS6 to DS3, seismic packages mostly show an aggradational arrangement with sigmoidal-oblique clinoforms (Fig. 12). At PS9 to PS10, which are thinner sequences, very few reflections can be distinguished, mostly at the bottomsets. The coral-coralline algal boundstone and foralgal floatstone to rudstone at the bottom of the succession corresponds to the upper part of the platform sequence ps9 (Fig. 12). Sequence ps9 is marked at this location by discontinuous, convex shaped reflections of medium amplitude gently inclined to the basin interior (Fig. 12).

The boundary PS10 seems to be the first one that delineates a late stage carbonate buildup on a palaeo upper slope of the platform. This buildup is represented through contorted, discontinuous reflections, sometimes with high-amplitude. The lower interval of the LBF packstone to grainstone and the coral boundstone are included in the platform sequence ps10. The seismic reflections in ps10 are similar to those of the underlying ps9 (Fig. 12) but slightly more chaotic in N-S view (Fig. 13).

PS11 is a thicker sequence with a topset of moderately continuous and discontinuous reflectors, locally convex up contorted. The deposits between ~304 and 227 mbsf correspond to the last platform sequence ps11 (Fig. 12). The sequence ps11 exhibits at the location of U1470, a package of slightly convex reflections of high amplitude gently inclined toward the basin. The lowermost and the uppermost reflections of the package coincide with the LBF packstone to grainstone and the mixed benthic foraminifera packstone and are moderately continuous (Fig. 12). In contrast, the reflections in the central part of this sequence are discontinuous and coincident with the mixed benthic foraminifera packstone interval (Fig. 12). No reflection terminations were identified throughout this seismic sequence. The change from the mixed benthic foraminifera packstone to the overlying foralgal floatstone to rudstone represents the sequence boundary DS1.

The overlying foralgal floatstone to rudstone, together with the LBF grainstone corresponds to the stratigraphic sequence ds1 (Fig. 4). This sequence is marked by sub-horizontal, moderately continuous reflections of high-amplitude inclined to the north and to the east (Figs. 12 and 13). At the DS1 boundary, in the central part of the analyzed N-S segment, the upper reflections of ps11 resemble erosional truncations at ca. 5000 and 7100 m (Fig. 13). The central parts of sequences DS1 to DS3 are eroded and form a depression, subsequently filled with younger drift deposits (Fig. 13). Drift sequences ds1 and ds2 include platform deposits only in their topsets and the upper parts of the foresets, while the bottomsets represents typical drift deposits (Fig. 12). A new package of foralgal floatstone marks the position of sequence boundary DS2. This facies alternates with coral-coralline algal boundstone intervals that constitute ds2. The stratigraphic sequence ds2 consists of continuous, slightly convex curved reflections of high amplitude. The contact of the foralgal floatstone with the overlying grainstone from the drift deposits is disturbed by drilling. This lithological change marks the base of the drift sequence ds3 (Figs. 12 and 13). Boundary DS3 represents the termination of the platform sedimentation. Above DS3, on the platform top drift sequences DS4 to DS6 merge together towards west.

5. Discussion

5.1 Facies interpretation

The texture and fossil assemblage of the different facies studied (table 1) together with the analysis of their equivalent seismic facies and its seismostratigraphic position (Figs. 10-13), allows for a palaeoenvironmental interpretation. The coral-coralline algal boundstone and the foralgal floatstone show abundant reef builders (Fig. 4) and seismic geometries with reflections changing from chaotic to relatively continuous and inclined toward the Inner Sea (Fig. 12). This indicates that these facies represent the transition from reef environments toward the forereef slope. The coralline algal assemblage, dominated by *Adeylithon* (=*Aethesolithon*) and *Neogoniolithon* is also indicative of shallow water reef environments. Extant *Adeylithon* thrives in shallow-water reef environments in the Pacific Ocean (Peña et al., 2018). *Aethesolithon* was established by Johnson (1964) in the Bonya Limestone, a Miocene forereef deposit in Guam (Schlanger, 1964). *Neogoniolithon* and *Adeylithon* (as *Aethesolithon*) are common genera in the middle Miocene shallow-water reef assemblages in East Kalimantan (Borneo) (Rösler et al., 2015), and Pleistocene reef deposits from NE Australia (Braga and Aguirre, 2004). The coarse-grained sediment and the predominance of thick-shelled *Amphistegin*a in the foralgal floatstone to rudstone are indicative of a high energy environment (Hallock and Glenn, 1986; Mateu-Vicens et al., 2009). *Amphistegina* has been reported as a common component in the upper reef-slopes in atolls of Java Sea (Renema, 2008). When the LBF are not dominant, the facies change into a rhodalgal rudstone mainly constituted by *Adeylithon*, characteristic of middle Miocene shallow-water reef deposits.

The LBF grainstone correlates to basinward dipping reflections at the platform margin that are interpreted as forereef slope deposits (Figs. 10 and 12). The low micrite content and the common fragmentation of *Cycloclypeus* and *Operculina* are indicators for an energetic environment such as the upper forereef slope (Tsuji, 1993; Hohenegger, 1994; Renema, 2008). The abundance of *Cycloclypeus,* typically dwelling in water depths from 50 m to the base of the photic zone ~120 m (Hohenegger et al., 1999, Hohenegger and Yordanova, 2001) or even deeper to 150 m (Tsuji, 1993), indicates that the deposition was probably at the deepest part of the upper slope. The great amount of corals also indicates proximity to the reef framework. Coralline algae appear as small, sand-sized fragments, which can be derived from shallower settings, such as the ones of *Adeylithon* and *Neogoniolithon,* or from plants that lived deeper on the slope, such as melobesiods and *Sporolithon*, characteristic of deeper assemblages (Bosence, 1991; Braga et al., 2010, Rösler et al., 2015). No consistent trend of relative abundance of shallow/deeper coralline assemblages can be observed.

The LBF packstone to grainstone and LBF floatstone to packstone correspond to gently inclined reflections than can be interpreted as the uppermost forereef slope (Fig. 12). The low micrite content and the abundance of thick-shelled forms of *Amphistegina* indicate deposition under relatively high-energy conditions (Hallock and Glenn, 1986; Mateu-Vicens et al., 2009).

The LBF rudstone contains a mixture of shallow dwellers, such as *Amphistegina*, and deeper dwellers, such as *Lepidocyclina*, *Cycloclypeus*, and *Operculina* (Hallock and Glenn, 1986; Tsuji, 1993, Hohenegger, 1994, Hohenegger et al., 1999, Hohenegger and Yordanova, 2001). The elongated and thick-shelled *Cycloclypeus* and *Operculina* together with large *Lepidocyclina* indicate that these facies were deposited in a relatively high-energy environment (Hohenegger and Yordanova, 2001, Renema et al., 2001; Mateu-Vicens et al., 2008). This is consistent with its seismostratigraphic position that place this facies at the forereef slope (Figs. 2 and 10).

The mixed benthic foraminifera floatstone to packstone with abundant small and large benthic foraminifera, such as miliolids, *Sorites*, *Marginopora*, *Borelis*, according to Beavington-Penney and Racey (2004) inhabit the upper part of a carbonate platform slope. *Sorites* is also reported to be abundant in reefs and upper reef slopes of Indonesia (Renema et al., 2001). This is consistent with seismic data showing basinward dipping reflections (Fig. 12). The preservation of *Borelis* and *Marginopora*, as well as the abundance of intraclasts may be interpreted as related to possible reworking of these components from adjacent areas. The remobilization of components by gravity processes is a common phenomenon at the upper part of carbonate platform slopes (Hine et al., 1992; Martinsen, 1994; Berra, 2007; Playton et al., 2010; Reolid et al., 2014; Reolid et al., 2017b). Downslope transport of modern foraminifera across a carbonate slope by storms and gravity processes has been reported as a common phenomenon in the Atlantic (Li et al., 1998) and in the Pacific (Vénec Peyré and Le Calvez, 1986; Hohenegger and Yordanova, 2001). All components of coralline assemblages occur in shallow-water reef environments in middle Miocene deposits in the Indo-Pacific as discussed above.

5.2 Carbonate platform evolution

Seismic data reveal that the Sites U1465 and U1470 penetrated sequences ps9 to ds2 at the top of the drowned Miocene platform (Betzler et al. 2016, 2018). The facies assemblage (Table 1) varies trough time from sequence to sequence and also laterally from the northern, Site U1465, to the southern, Site U14710, branch of the WKC (Fig. 1).

5.2.1 Sequence ps9

Platform sequence ps9 was exclusively recovered in the southern branch of the WKC. The coral-coralline algal boundstone and the foralgal floatstone corresponding to ps9 overlie the platform edge marked by sequence boundary PS9. The coral-coralline algal boundstone and the foralgal floatstone (Fig. 4) and the seismic geometries (Fig. 12) indicate deposition at the reef and forereef slope environments. The estimated palaeodepth derived from the platform geometry places these deposits around 20-30 m depth, considering the platform top at sea level (Fig. 12).

5.2.2 Sequence ps10

In the southern Site U1470, this sequence is characterised by foralgal floatstone to rudstone and LBF packstone to grainstone corresponding to gently inclined reflections than can be interpreted as the uppermost forereef slope of ps10 (Fig. 12). The estimated depth based on the seismic profiles suggests deposition around 50 m depth (Fig. 12).

In the northern Site U1465, the LBF grainstone is interpreted as the proximal forereef slope (Fig. 10). No consistent trend of relative abundance of shallow/deeper coralline or LBF assemblages can be observed. The only indicator of palaeobathymetry is the up-core decrease in *Miogypsina* (Fig. 2), indicative of a progressive deepening of the environment, as *Miogypsina* prefers shallow, warm waters (Chaproniere, 1984; Hallock and Glenn, 1986). The change from LBF grainstone to LBF packstone to grainstone at 163 mbsf indicates an environment progressively less energetic (Fig. 2). The interpretation of these packages as lowstand wedge and the following transgressive deposits is consistent with the progressive deepening suggested by the diminishing amount of *Miogypsina* that disappear at 163 mbsf coinciding with the base of the overlying highstand package. The LBF packstone and the intercalated LBF rudstone represents the forereef facies. The relatively scarce fragmentation of the LBF and the presence of some thin-shelled *Cycloclypeus* point to a sheltered place where shallow and deeper dwellers biota accumulate in-situ or with little transport. Thus, this facies may represent relatively protected areas at the upper platform slope.

5.2.3 Sequence ps11

In the southern Site U1470, this sequence is characterised by a lower part of LBF packstone to grainstone with relatively continuous reflections gently dipping to the basin, which can be interpreted as the upper platform slope (Fig. 12). The overlying mixed benthic foraminifer floatstone shows stained bioclasts and abundant intraclasts that may be interpreted as possible redeposition of these components from adjacent areas. This is consistent with the occurrence of this facies adjacent to the shallow trough imaged in N-S view (Fig. 13). The estimated depth of deposition varies from approximately 60 m at the base of the sequence to around 30-40 to the top (Fig. 12).

At the northern Site U1465, ps11 consists of a thick interval of LBF packstone to grainstone with an intercalated LBF floatstone to packstone that were deposited accordingly to the seismostratigraphy at the upper forereef slope (Fig. 2). The occurrence of reefal components as corals encrusted by red algae, bryozoans, and foraminifera is consistent with proximity to the reef. The overlying foralgal floatstone to rudstone correlates to sub-parallel to chaotic reflections dipping toward the basin interior that may represent the uppermost forereef slope (Figs. 2 and 10). This interpretation is in line with the depth estimation based on the seismic profiles suggesting that deposition in ps11 start around 70 m depth and was shallowing until deposition approximately at sea level (Fig. 11). It should be noted that the platform at the position of Site U1465 is eroded, at least 10-20 m with respect to adjacent areas (Fig. 10). In any case, the shallowing during the deposition of ps11 is corroborated by the occurrence of geopetal structures at the top of the sequence (Fig. 8). The occurrence of micrite infilling the molds of previously dissolved bioclasts is a clear indicator of karstification (Sanford and Konikow, 1989; Budd, 1992; Swart, 2015; Reolid et al., 2016). The subaerial exposure of the upper part of the carbonate platform triggered the dissolution of the aragonitic components (Swart, 2015). Subaerial exposure is also proposed as the cause of the extensive dolomitization observed at Site U1469 (Prince et al., in prep). A later flooding of the platform top allowed the deposition of micrite in the molds. The occurrence of *Gastrochaenolites* (trace of boring bivalves) at the top of the interval (Table 1) is consistent with a depositional break. At the location of Site U1465 the estimated hiatus is of up to 6 Myr (Lüdmann et al., 2018).

5.2.4 Sequence ds1

Platform facies in sequence ds1 only occur in the southern part of the WKC. The foralgal floatstone to rudstone were deposited in at least 40 m of water depth, this is in line with deposition in the upper slope (Fig. 11). The overlying LBF grainstone occurring together with basinward dipping reflections at the platform margin is interpreted as the deposits of the forereef slope (Fig. 12). The increased amount of *Cycloclypeus*, and the presence of coralline algae, including melobesiod and *Sporolithon* fragments, suggest an environment of depth similar to that of the previous interval (Bosence, 1991; Braga et al. 2010).

5.2.5 Sequence ds2

The platform facies in ds2 only developed at the southern Site U1470 and consists of a foralgal floatstone with intercalations of coral-coralline algal boundstone (Fig. 2). These facies are interpreted above as reef and adjacent deposits. While the boundstone is clearly interpreted as a reef, the foralgal floatstone may be identified as a forereef deposit close to the reef itself, based on the basinward-dipping continuous reflections equivalent to the foralgal floatstone point to deposition in the forereef slope close to the reef itself (Fig. 12). This interpretation is congruent with the water depth estimated from of the seismic profiles, which changes from 30 m to around 0 m at the top of ds2 (Fig. 12).

5.3 Stepwise drowning of the Miocene platform

Betzler et al. (2009, 2013, 2016, 2017, 2018) and Lüdmann et al. (2013) were the first to connect the partial drowning of the Miocene carbonate platform of the Maldives with the onset of the South Asian Monsoon in the Indian Ocean. According to these authors, the drowning of the carbonate edifice was attributed to the input of nutrients by upwelling produced by the Monsoon winds and also to the physical effects of currents.

During the early Miocene, sea-level controlled the stacking pattern and facies distribution in the carbonate platform and the slope deposits of the Maldives (Betzler et al., 2009; 2013; 2016; 2018). The lowest sea-level position of the Miocene recorded in the studied succession occurs at the top of ps11 when aragonitic and high-Mg calcite components were dissolved during karstification (Fig. 8). The later reflooding of the platform top promoted the colonization by boring organisms (*Gastrochaenolites*) (Table 1). Palaeowater depth eventually increased as recorded by the occurrence of small planktonic foraminifera and micrite within the geopetal infills of some molds (Fig. 8). The reflooding resulted in the drowning of the platform, when strong currents swept the platforms preventing the re-establishment of shallow-water ecosystems and caused the demise of this platform segment, and many others throughout the Maldives (Betzler et al., 2009, 2016). According to numerical modelling based on present day coral-reef dynamics, strong currents may increase the supply of material by erosion and the duration of these materials in resuspension, harming the conditions for a normal development of coral reefs (Storlazzi et al., 2011). Currents are also proved to have a negative effect on the settlement of coral larvae (Stoner, 1990). Strong off-bank currents, as those of the Maldives around 13 Ma, likely swept coral larvae away from the platform to unfavourable habitats where they finally settled down and died, as it occurs in present day reefs (Stoner, 1990; Fraschetti et al., 2002). The strength of the currents had two consequences: the mechanical erosion at the platform top that produced a stratigraphic hiatus of circa 6 Myr (Lüdmann et al., 2018), and the accumulation of sediment in the basin interior forming a delta drift (Lüdmann et al., 2018; Reolid et al., 2019). These invigorated currents are the result of the onset of the South Asian Monsoon (Betzler et al., 2016, 2018).

The equivalent platform deposits at the southern branch of the WKC, at Site U1470 are dominated by slope packstone and grainstone, in contrast to the reefal boundstone and floatstone of Site U1465, which suggests deposition in a deeper environment. The facies in the southern site also lack features reflecting subaerial exposure as in the northern site. The falling sea level in this area is probably imaged by the shallow trough observed in seismic profiles (Fig. 13) and the abundance of intraclasts and reworked bioclasts in mixed benthic foraminifera floatstone (Table 1).

In the north, the later reflooding of the platform brought strong currents that hindered the platform regeneration and the concomitant drift deposition in the Inner Sea and the flanks of the atolls (Fig. 10; Betzler et al. 2009, 2013, 2016; Lüdmann et al. 2013; Lüdmann et al., 2018; Reolid et al., 2019), in contrast in the south the carbonate platform grew at the same time drift deposition occurred in the basin (Figs. 12 and 13). Thus, the platform developed under the influence of currents, but presumably not as strong as in the northern site according to the minor erosion of the platform top (Figs. 10 and 12). The southern branch of the WKC was sensibly smaller and less energetic that the northern one (see Figure 7 of Lüdmann et al., 2018). This allowed for the coexistence of an active platform exporting sediment downslope together with current-controlled deposits in the basin resulting in some peculiarities of the drift deposits in the southern Kardiva Channel. Reolid and Betzler (2018, 2019) showed that ichnofabrics display an abrupt increase in the intensity of bioturbation when changing from slope to drift deposits. In the northern Kardiva Channel this change is sharp and coincides with DS1 (Reolid and Betzler, 2019). In contrast, in the southern Kardiva Channel, slope ichnofabrics alternate with drift ichnofabrics between DS1 and DS3, until being completely replaced by typical drift ichnofabrics at DS3. Both, carbonate platform and drift deposits were apparently balanced during the time span between DS1 and DS3. Finally, the sea-level fall at 10.6 Ma likely destroyed the equilibrium between both depositional systems in favour of the current-controlled deposits. Betzler et al. (2018) reported that DS3 is the only drift sequence boundary that is coincident with a global sea-level lowstand. Here it is proposed that this sea-level lowstand promoted the harming of the carbonate platform that leaded to its later drowning in the southern part of the Kardiva Channel in the same way the sea-level fall predating DS1 did in the north.

Finally, the input of nutrient should be considered as secondary factor contributing to the drowning of the Miocene carbonate platform of the Maldives. The negative influence of nutrients on reef communities, together with sea-level fluctuations, is typically considered as one of the causes of reef drowning (Hallock and Schlager, 1986). Numerous studies focus on how fossil assemblages change when nutrient-rich waters reach carbonate platforms (Hallock and Schlager, 1986; Hallock et al., 1991; Wood, 1993, 1995; Mutti and Hallock, 2003; Sattler et al., 2009). However, no palaeontological or sedimentological evidences point to a significant role of nutrients in the drowning of this carbonate platform.

In the southern branch of the Kardiva Channel, the first input of bottom currents from the Indian Ocean is marked by DS1 and the start of the drift deposition, but the carbonate platform prior and after this event displays a similar fossil assemblage (Fig. 2) with only minor changes resulting of the rising sea level. The nitrogen isotopes (δ^{15}N), total organic carbon (TOC), and the improved phosphorus sequential extraction (SPExMan-SEDEX) were also studied in this interval in order to evaluate the role of nutrients on the platform drowning (Ling et al., in this volume). These nutrient proxies, δ^{15}N and phosphorus (P), reveal that the nutrient content across the drowning success=sion remain stable during the onset of the wind-driven currents (Ling et al., in this volume). In addition, little to no TOC is preserved in the sediments across the drowning successions (Ling et al., in this volume). Thus, it is proposed that the drowning of the Miocene carbonate platform of the Maldives was the result of the combined effect of intensified oceanic currents and the fluctuating sea level alone.

6. Conclusions

The study of the carbonate platform of the Maldives shows that the Miocene drowning was not coeval throughout the Maldives. The main drowning phase for most of the Maldives edifice, and especially in the northern branch of the western Kardiva Channel, occurred at 13 Ma and it is marked by the distinctive sequence boundary. In contrast, the carbonate platform in the southern branch of the western Kardiva Channel was drowned at 10.6 Ma, circa 2 Myr later than the rest of the Maldives.

The carbonate platform interval in the northern branch of the Kardiva Channel consists of a succession of slope and reef facies overlain by drift deposits. The top of the carbonate platform displays evidences of subaerial exposure related to a global sea-level fall that predated the main drowning event. The reflooding of the platform at 13 Ma came together with the establishment of strong currents that eroded the platform top and promoted the drift deposition in the basin interior.

The carbonate platform in the southern branch of the Kardiva Channel does not show evidences of subaerial exposure. The installation of currents started the drift the deposition in the basin at 13 Ma, however the currents were weaker than in the northern branch and allows for the development of a carbonate platform coeval to the drift deposits that coexisted for circa 2 Myr. The global sea-level fall at 10.6 Ma and the later reflooding of the platform likely destroyed the equilibrium between both depositional systems in favour of the current-controlled deposits.

The fossil assemblages in the carbonate platform prior and after the main drowning event at 13 Ma are similar and do not show evidence of significant increase in nutrient input, as frequently documented in other drowned carbonate platforms elsewhere. It is proposed that the drowning of the Miocene carbonate platform of the Maldives was the result of the combined effect of the fluctuating sea level during the Neogene and the intensification of oceanic currents due to the invigoration of the South Asian Monsoon.

Acknowledgments

This research used samples and data provided by the International Ocean Discovery Program (IODP). This study would not have been possible without the dedicated effort of the drilling crew, ship's crew and scientific staff of the Drillship JOIDES Resolution during IODP Exp. 359. CB, TL, and JR thank the DFG for funding the project INDOCARB (Be1272/23-1 and Be1272/23-2). JR thanks the MINECO of Spain for personal funding through the Juan de la Cierva Program. JCB and JR are thankful for funding from research group RNM-190. Many discussions with the IODP Exp. 359 shipboard scientists helped us to sharpen our concept. Catalina Vulpe is thanked for his work with the microfacies. Additional acknowledgements go to the companies Halliburton-Landmark, Schlumberger and Cegal Geosciences for providing university grants for the seismic processing software PROMAX and seismic interpretation software PETREL as well as its BLUEBACK plugin. Eva Vinx is thanked for the production of the many thin sections. All authors want to acknowledge an anonymous reviewer, as well as Guest Editor Dr. Jeremy Young and Editor Dr. Thomas Algeo for their valuable comments that helped to improve the final version of this manuscript.

References

Arthur, M.A., Schlager, S.O., 1979. Cretaceous "oceanic anoxic events" as causal factors in development of reef-reservoired giant oil fields. AAPG Bull. 63, 870–885.

Aubert, O., Droxler, A.W., 1992. General Cenozoic evolution of the Maldives carbonate system (equatorial Indian Ocean). Bull. Centres Rech. Explor.-Prod. Elf-Aquitaine 16, 113–136.

Beavington Penney, S.J., Racey, A., 2004. Ecology of extant nummulitids and other larger benthic foraminifera; applications in palaeoenvironmental analysis. Earth Science Reviews 67, 219–265.

Belopolsky, A., Droxler, A.W., 2003. Imaging Tertiary Carbonate System - the Maldives, Indian Ocean: Insights into Carbonate Sequence Interpretation. Lead. Edge 22, 646–652.

Belopolsky, A., Droxler, A.W., 2004a. Seismic expressions of prograding carbonate bank margins: Middle Miocene, Maldives, Indian Ocean. In: Seismic Imaging of Carbonate Reservoirs and Systems (Ed G.P. Eberli, J.L. Masaferro, and J.F. Sarg), AAPG Mem., 81, 267–290.

Belopolsky, A., Droxler, A.W., 2004b. Seismic expressions and interpretation of carbonate sequences: the Maldives platform, equatorial Indian Ocean. AAPG, Stud. Geol. 49, 1–46.

Berra, F., 2007. Sedimentation in shallow to deep water carbonate environments across a sequence boundary: effects of a fall in sea-level on the evolution of a carbonate system (Ladinian-Carnian, eastern Lombardy, Italy). Sedimentol. 54, 721–735.

Betzler, C., Hübscher, C., Lindhorst, S., Reijmer, J.J.G., Römer, M., Droxler, A., Fürstenau, J., Lüdmann, T., 2009. Monsoon-Induced Partial Carbonate Platform Drowning (Maldives, Indian Ocean). Geol. 37, 867–870.

Betzler, C., Lüdmann, T., Hübscher, C., Fürstenau, J., 2013. Current and Sea-Level Signals in Periplatform Ooze (Neogene, Maldives, Indian Ocean). Sed. Geol. 290, 126–137.

Betzler, C., Eberli, G.P., Kroon, D., Wright, J.D., Swart, P.K., Nath, B.N., Alvarez-Zarkikian, C.A., Alonso-Garcia, M., Bialik, O.M., Blatter, C.L., Guo, J.A., Haffen, S., Horozal, S., Inoue, M., Jovane, L., Lanci, L., Laya, J.C., Mee, A.L., Lüdmann, T., Nakakuni, M., Niino, K., Petruny, L.M., Pratiwi, S.D., Reijmer, J.J.G., Reolid, J., Slagle, A.L., Sloss, C.R., Su, X., Yao, Z., Young, J.R., 2016. The Abrupt Onset of the Modern South Asian Monsoon Winds. Sci. Rep. 6, 29838.

Betzler, C., Eberli, G.P., Alvarez-Zarikian, C.A. and the Expedition 359 Scientists, 2017. Maldives Monsoon and Sea Level. Proceedings of the International Ocean Discovery Program, 359: College Station, TX (International Ocean Discovery Program). http://dx.doi.org/10.14379/iodp.proc.359.2017

Betzler, C., Eberli, G.P., Lüdmann, T., Reolid, J., Kroon, D., Reijmer, J.J.G., Swart, P.K., Wright, J., Young, J.R., Alvarez-Zarikian, C., Alonso-García, M., Bialik, O.M., Blättler, C.L., Guo, J.A., Haffen, S., Horozal, S., Inoue, M., Jovane, L., Lanci, L., Laya. J.C., Hui Mee, A.L., Nakakuni, M., Nath, B.N., Niino, K., Petruny, L.M., Pratiwi, S.D., Slagle, A.L., Sloss, C.R., Su, X., Yao, Z., 2018. Refinement of Miocene sea-level and monsoon events from the sedimentary record of the Maldives (Indian Ocean). Progress in Earth and Planetary Science. DOI 10.1186/s40645-018-0165-x

Bosence, D.W.J., 1991. Coralline algae: mineralization, taxonomy and palaeoecology. In: Calcareous algae and stromatolites (Ed R. Riding). Springer, Berlin, 98–113.

Braga, J.C., Aguirre, J., 2004. Coralline algae indicate Pleistocene evolution from deep, open platform to outer barrier reef environments in the northern Great Barrier Reef margin. Coral Reefs 23, 547–558.

Braga, J.C., Bassi, D., Piller, W.E., 2010. Paleoenvironmental significance of Oligocene-Miocene coralline red algae – a review. In: Carbonate system during the Oligocene-Miocene Climatic Transition (Eds M. Mutti, W.E. Piller, and C. Betzler). Int. Assoc. Sedimentol. Spec. Publ. 42.

Budd, D.A., 1992. Dissolution of high-Mg calcite fossils and the formation of biomolds during mineralogical stabilization. Carbonates and Evaporites 7, 74–81.

Burchette, T.P., 2012. Carbonate rocks and petroleum reservoirs: A geological perspective from the industry. Geol. Soc. of London, Spec. Pub. 370(1), 17–37.

Chaproniere, G.C., 1984. The Neogene larger foraminiferal sequence in the Australian and New Zealand regions, and its relevance to the East Indies letter stage classification. Palaeogeog., palaeoclimatol., palaeoecol. 46(1-3), 25– 35.

Duncan, R.A., Hargraves, R.B., 1990. $^{40}Ar/^{39}Ar$ geochronology of basement rocks from the Mascarene Plateau, the Chagos Bank, and the Maldives Ridge. In: Scientific Results (Eds R.A. Duncan, J. Backman, and L.C. Peterson), Proceedings of the Ocean Drilling Program 115, 43–51.

Dunham, R. J., 1962. Classification of carbonate rocks according to depositional texture, in W.E. Ham, ed., Classifications of carbonate rocks-a symposium: AAPG Memoir 1, 108–121.

Eberli, G.P., 1991. Growth and demise of isolated carbonate platforms: Bahamian controversies. Controversies in Modern Geology 231–248.

Eberli, G.P., Anselmetti, F.S., Isern, A.R., Delius, H., 2010. Timing of changes in sea-level and currents along the Miocene platforms of the Marion Plateau, Australia. In: Cenozoic Carbonate Systems of Australasia (Eds W.A. Morgan, A.D. George, P.M. Harris, J.A. Kupecz and J.E: Sarg J.E.), SEPM Spec. Publ. 95, 219–242.

Embry, A.F., Klovan, J.E., 1972. Absolute water depth limits of Late Devonian paleoecological zones. Geologische Rundschau 61, 672–686.

Erlich, R.N., Barrett, S.F., Ju, G.B., 1990. Seismic and Geologic characteristics of drowning events on carbonate platforms (1). AAPG Bull. 74(10), 1523– 1537.

Fraschetti, S., Giangrande, A., Terlizzi, A., Boero, F., 2002. Pre- and post-settlement events in benthic community dynamics. Oceanologica Acta 25, 285–295.

Hallock, P., Premoli-Silva, I., Boersma, A., 1991. Similarities between planktonic and larger foraminiferal evolutionary trends through Paleogene paleoceanographic changes. Palaeogeogr. Palaeoclimat. 83, 49–64.

Hallock, P., Glenn, E.C., 1986. Larger foraminifera: a tool for paleoenvironmental analysis of Cenozoic carbonate facies. Palaios 1, 55–64.

Hallock, P., Schlager, W., 1986. Nutrient excess and the demise of coral reefs and carbonate platforms. Palaios 1, 389–398.

Hine, A.C., Locker, S.D., Tedesco, L.P., Mullins, H.T., Hallock, P., Belknap, D.F., Gonzales, J.L., Neumann, A.C., Snyder, S.W., 1992. Megabreccia shedding from modern, low relief carbonate platforms, Nicaraguan Rise. Geol. Soc. of America Bull. 104, 928–943.

Hohenegger, J., Yordanova, E., Nakano, Y., Tatzreiter, F., 1999. Habitats of larger foraminifera on the upper reef slope of Sesoko Island, Okinawa, Japan. Mar. Micropaleontol. 36, 109–168.

Hohenegger, J., 1994. Distribution of living larger foraminifera NW of Sesoko Jima, Okinawa, Japan. Mar. Ecol. 15, 291–334.

Hohenegger, J., Yordanova, E., 2001. Displacement of larger foraminifera at the western slope of Motobu peninsula (Okinawa, Japan). Palaios 16, 53–72.

Johnson, J.H., 1964. Fossil and recent calcareous algae from Guami. U.S. Geol. Surv. Prof. Pap. 403-G, 1–40.

Li, C., Jones, B., Kalbfleisch, W.B.C., 1998. Carbonate sediment transport pathways based on foraminifera: Case study from Frank Sound, Grand Cayman, British West Indies: Sedimentol. 45, 109–120.

Ling, A., Ebreli, G.P., Swart, P.K., Hayman, S., Ruggenberg, A., Betzler, C., Reolid, J., in this volume. The influence of nutrient excess and the Oxygen Minimum Zone (OMZ) on the partial drowning of the Kardiva Platform (Mid-Miocene, Maldives). Palaeogeogr. Palaeoclimatol. Palaeoecol.

Lüdmann, T., Kalvelage, C., Betzler, C., Fürstenau, J., Hübscher, C., 2013. The Maldives, a Giant Isolated Carbonate Platform Dominated by Bottom Currents. Mar. Petrol. Geol. 43, 326–340.

Lüdmann, T., Betzler, C., Eberli, G.P., Reolid, J., Reijmer, J.J.G., Sloss, C.R., Bialik, O.M., Alvarez-Zarkikian, C.A., Alonso-Garcia, M., Blatter, C.L., Guo, J.A., Haffen, S., Horozal, S., Inoue, M., Jovane, L., Kroon, D., Lanci, L., Laya, J.C., Mee, A.L., Nakakuni, M., Nath, B.N., Niino, K., Petruny, L.M., Pratiwi, S.D., Slagle, A.L., Su, X., Swart, P.K., Wright, J.D., Yao, Z., Young, J.R., 2018. Carbonate delta drifts: a new drift type. Mar. Geol. 401, 98–111.

Martinsen, O. (1994) Mass movements. In: The Geological Deformation of Sediments (Ed. A. Maltman). Chapman & Hall, London, 127–165.

Mateu-Vicens, G., Hallock, P., Brandano, M., 2009. Test-shape variability of Amphistegina d'Orbigny, 1826 as a paleobathymetric proxy: application to two Miocene examples. In: Geologic Problem Solving with Microfossils: A Volume in Honor of Garry D. Jones (Eds T. Demchuk and A. Gary), SEPM Spec. Publ. 93, 67–82.

Mitchum, R.M., Vail, P.R., Sangree, J.B., 1977. Seismic stratigraphy and global changes of sea level: Part 6. Stratigraphic interpretation of seismic reflection patterns in depositional sequences. In: Seismic stratigraphy—applications to hydrocarbon exploration (Ed C.E. Payton). AAPG Bull. 26, 117–134.

Mutti, M., Hallock, P., 2003. Carbonate systems along nutrient and temperature gradients: Some sedimentological and geochemical constraints. Int. J. Earth Sci. 92, 465–475.

Peña, V., Le Gall, L., Rösler, A., Payri, C.E., Braga, J.C., 2018. *Adeylithon* bosencei gen. et sp. nov. (Corallinales, Rhodophyta): a new reef-building genus with anatomical affinities with the fossil *Aethesolithon*. Journal of Phycology, doi: 10.1111/jpy.12799

Playton, T.E., Janson, X., Kerans, C., 2010. Carbonate slopes. In: Facies Models 4, GEOtext 6: Geological Association of Canada (Eds N.P. James and R.W. Dalrymple). St John’s, Newfoundland, 449–476.

Prince, K., Laya, J.C., Betzler, C., Reolid, J., Lüdmann, T., Swart, P.K., Blättler, C.L., Miller, B.V., in this volumen. Sea Level and Current Dominated Diagenetic Regimes of the Kardiva Platform, Maldives. Palaeogeogr. Palaeoclimatol. Palaeoecol.

Purdy, E.G., Bertram, G.T., 1993. Carbonate Concepts from the Maldives, Indian Ocean. AAPG Studies in Geology, 34, 56 pp.

Renema, W., 2008. Habitat selective factors influencing the distribution of larger benthic foraminiferal assemblages over the Kepulauan Seribu. Mar. Micropaleontol. 68, 286–298.

Renema, W., Troelstra, S.R., 2001. Larger foraminifera distribution on a mesotrophic carbonate shelf in SW Sulawesi (Indonesia). Palaeogeogr. Palaeoclimatol. Palaeoecol. 175, 125–146.

Reolid, J., Betzler, C., 2018. Ichnofabrics logs for the characterization of the organic content in carbonates. Mar. Petrol. Geol. 95, 246–254.

Reolid, J., Betzler, C., 2019. The ichnology of carbonate drifts. Sedimentol. https://doi.org/10.1111/sed.12563

Reolid, J., Betzler, C., Braga, J.C., Martín, J.M., Lindhorst, S., Reijmer, J.J.G., 2014. Reef Slope Geometries and Facies Distribution: Controlling Factors (Messinian, SE Spain). Facies 60, 737–753.

Reolid, J., Betzler, C., Braga, J.C, 2016. Amplitude of late Miocene sea-level fluctuations from karst development in reef-slope deposits (SE Spain). Sedimentary Geol. 345, 145–153.

Reolid, J., Reolid, M., Betzler, C., Lindhorst, S., Wiesner, M. G., Lahajnar, N., 2017a. Upper Pleistocene cold-water corals from the Inner Sea of the Maldives: taphonomy and environment. Facies 63:11, 1–20.

Reolid, J., Betzler, C., Singler, V., Stange, C., Lindhorst, S., 2017b. Facies variability in mixed carbonate-siliciclastic platform slopes (Miocene). Facies 63:11, 2–19.

Reolid, J., Betzler, C., Lüdmann, T., 2019. Facies and sedimentology of a carbonate delta drift (Miocene, Maldives). Sedimentol. https://doi.org/10.1111/sed.12575

Rösler, A., Pretkovic, V., Novak, V., Renema, W., Braga, J.C., 2015. Coralline algae from the Miocene Mahakam Delta (East Kalimantan, SE Asia). Palaios 30, 83–93.

Sanford, W.E., Konikow, L.F., 1989. Porosity development in coastal carbonate aquifers. Geol. 17, 249–252.

Sattler, U., Immenhauser, A., Schlager, W., Zampetti, V., 2009. Drowning history of a Miocene carbonate platform (Zhujiang Formation, South China Sea). Sedimentary Geol. 219, 318–331.

Schlager, W., 1981. The paradox of drowned reefs and carbonate platforms. Geol. Soc. of America 92, 197–211.

Schlager, W., 1989. Drowning unconformities on carbonate platforms. In: Controls on Carbonate Platform and Basin Development (Eds P.D. Crevello, J.L.cWilson, J.F. Sarg, and J.F. Read). SEPM Spec. Pub. 44, 15–26.

Schlager, W., Camber, O., 1986. Submarine slope angles, drowning unconformities, and self-erosion of limestone escarpments. Geol. 14, 762–765.

Schlanger, S.O., 1964. Petrology of the limestones of Guam. U.S. Geol. Surv. Prof. Pap., 403-D: Dl–D52.

Stoner, D.S., 1990. Recruitment of a tropical colonial ascidian relative importance of pre-settlement vs post-settlement processes. Ecol. 7, 1682– 1690.

Storlazzi, C.D., Elias, E., Field, M.E., Presto, M.K., 2011. Numerical modeling of the impact of sea-level rise on fringing coral reef hydrodynamics and sediment transport. Coral Reefs 30, 83– 96.

Swart, P.K., 2015, The geochemistry of carbonate diagenesis: The past, present and future. Sedimentol. 62, 1233–1304.

Tsuji, Y., 1993. Tide influenced high energy environments and rhodolith-associated carbonate deposition on the outer shelf and slope off the Miyako Islands, southern Ryukyu Island Arc, Japan. Mar. Geol. 113, 255–271.

Vénec-Peyré, M.T., Le Calvez, Y., 1986. Foraminifères benthiques et phénomènes de transfert: Importance des études comparatives de la biocenose et de la thanatocénose: Bulletin du Muséum d'Histoire Naturelle, Paris, 8, 171–184.

Weissert, H., Lini, A., Föllmi, K.B., Kuhn, O., 1998. Correlation of Early Cretaceous carbon isotope stratigraphy and platform drowning events: A possible link? Palaeogeogr. Palaeoclimatol. Palaeoecol. 137, 189–203.

Wilson, M.E.J., Hall, R., 2010. Tectonic influences on SE Asian carbonate systems and their reservoir development. In: Cenozoic Carbonate Systems of Australasia (Eds W.A. Morgan, A.D. George, P.M. Harris, J.A. Kupecz and J.E: Sarg J.E.), SEPM Spec. Publ. 95, 13–40.

Wood, R., 1993. Nutrients, predation and the history of reef-building. Palaios 8, 526–543.

Wood, R., 1995. The changing biology of reef building. Palaios 10, 517–529.

Figures:

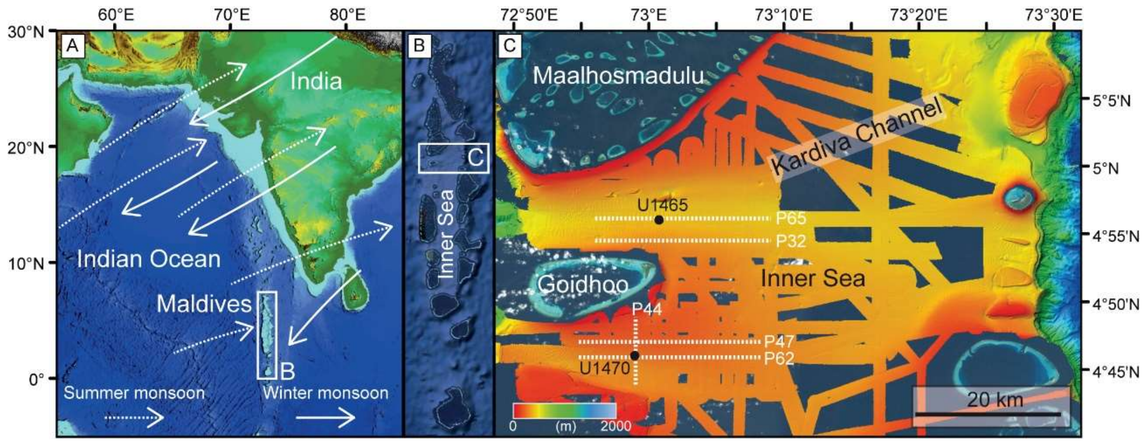

Figure 1

Figure 1: Map of the study area in the northern part of the Maldives (modified after Lüdmann *et al.*, 2018). (A) Location of the Maldives in the Indian Ocean. (B) Location of the study area in the northern part of the Maldives. (C) Location of IODP Expedition 359 Sites U1465 and U1470. Dashed lines represent the seismic lines displayed in Figures

9 to 12.

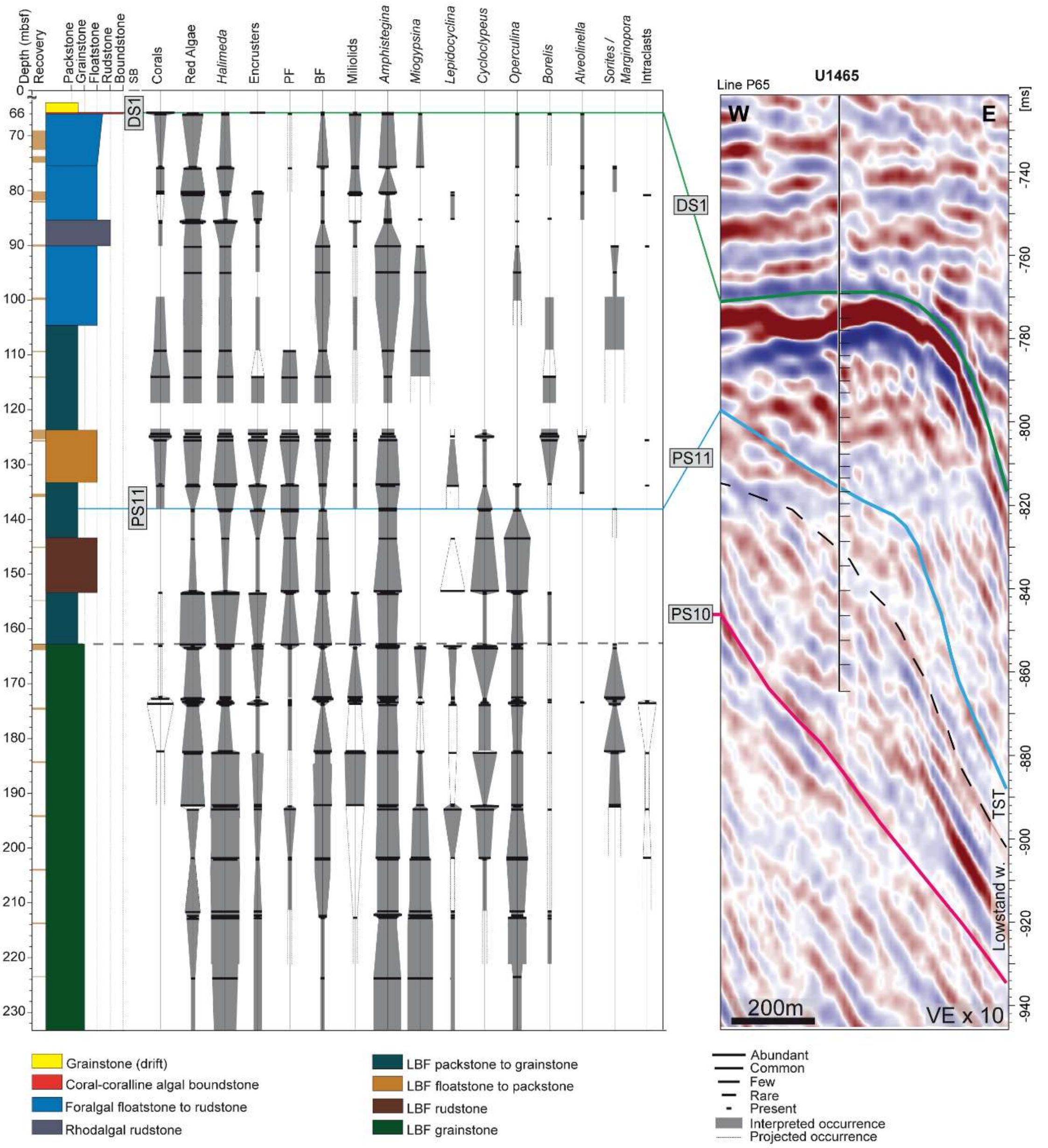

Figure 2

Figure 2: Lithological column of the platform and platform slope deposits at Site U1465 including from left to right: depth (mbsf), recovery, carbonate texture, sequence boundary, components, and reflection-seismic profile. In the seismic profile ps10 is separated in a lowstand wedge and the overlying transgressive deposits (TST).

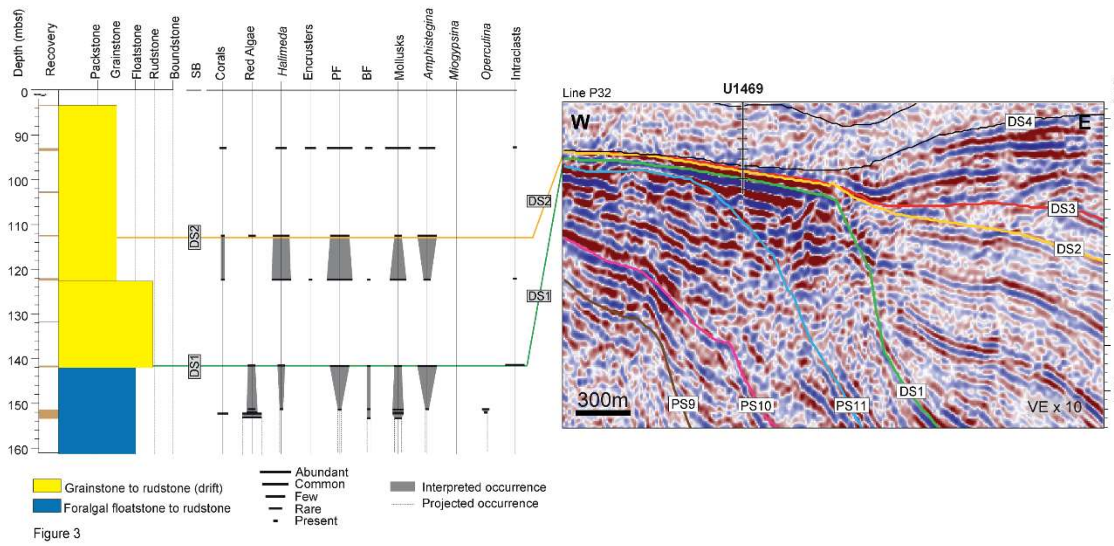

Figure 3: Lithological column of the platform and platform slope deposits at Site U1469 including from left to right: depth (mbsf), recovery, carbonate texture, sequence boundary, components, and reflection-seismic profile.

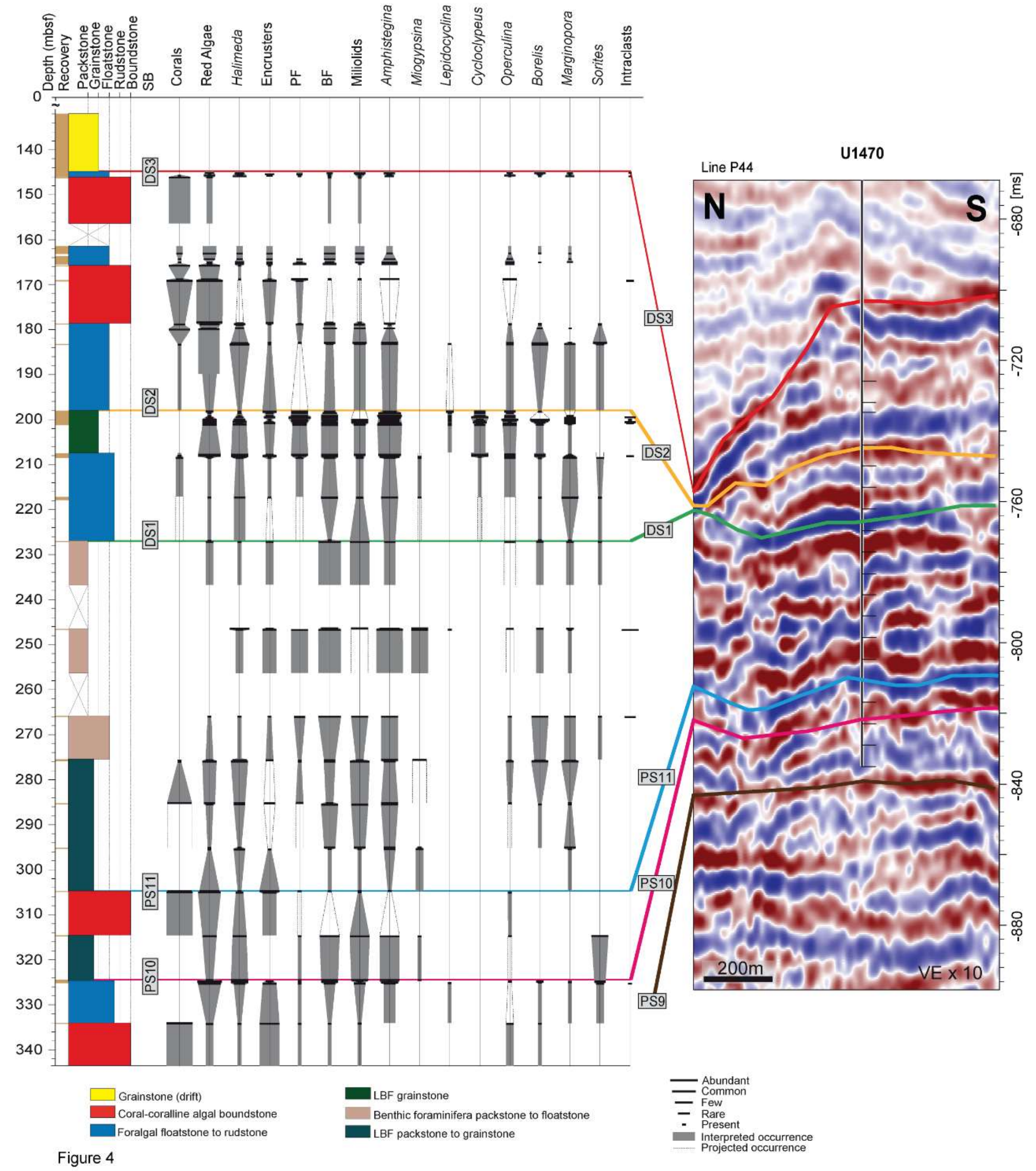

Figure 4

Figure 4: Lithological column of the platform and platform slope deposits at Site U1470 including from left to right: depth (mbsf), recovery, carbonate texture, sequence boundary, components, and reflection-seismic profile.

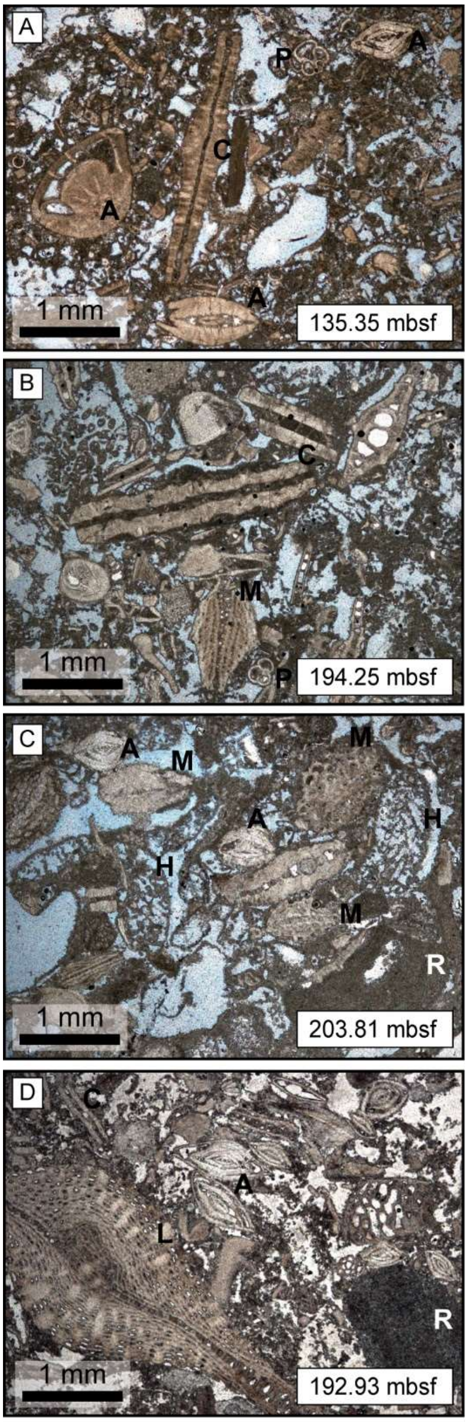

Figure 5

Figure 5: Photomicrographs of the different upper slope facies ordered by their micritic content: (A) LBF packstone, (B) LBF packstone to grainstone, (C) LBF grainstone to packstone, and (D) LBF grainstone to rudstone. A = *Amphistegina*, C = *Cycloclypeus*, H = *Halimeda* plate, L = *Lepidocyclina*, M = *Miogypsina*, P = planktonic foraminifera, and R = Red algae.

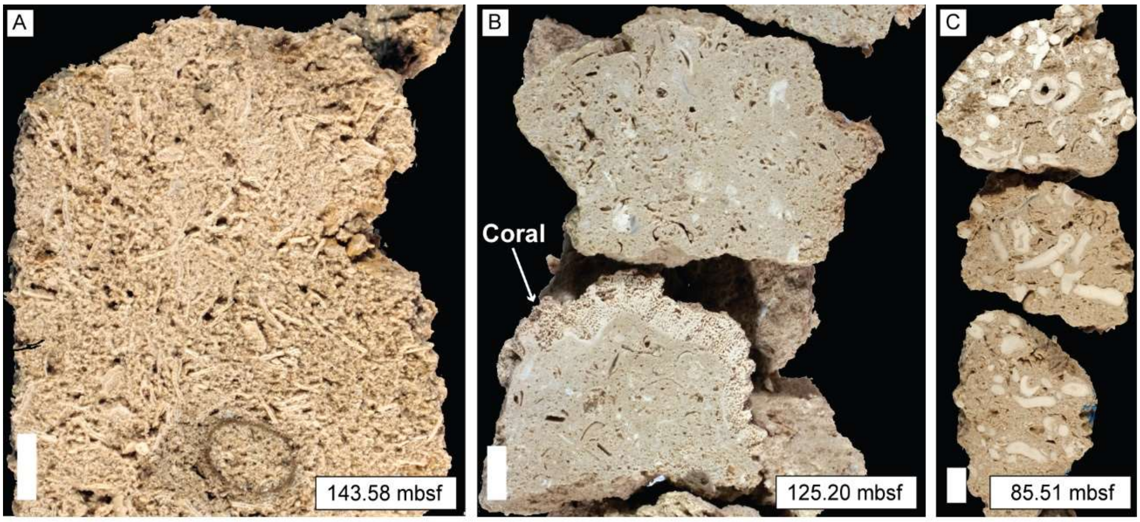

Figure 6

Figure 6: Coarse-grained facies of the platform slope deposits. (A) LBF rudstone with abundant *Cycloclypeus* (long tests) and *Amphistegina* (rounded tests). (B) LBF packstone to floatstone with common fragments of corals, mollusks, and red algae. (C) Rhodalgal floatstone with abundant red algae fragments and some mollusk fragments.

Figure 7

Figure 7: Core photographs of the foralgal floatstone at Site U1465 (A) and U1470 (B).

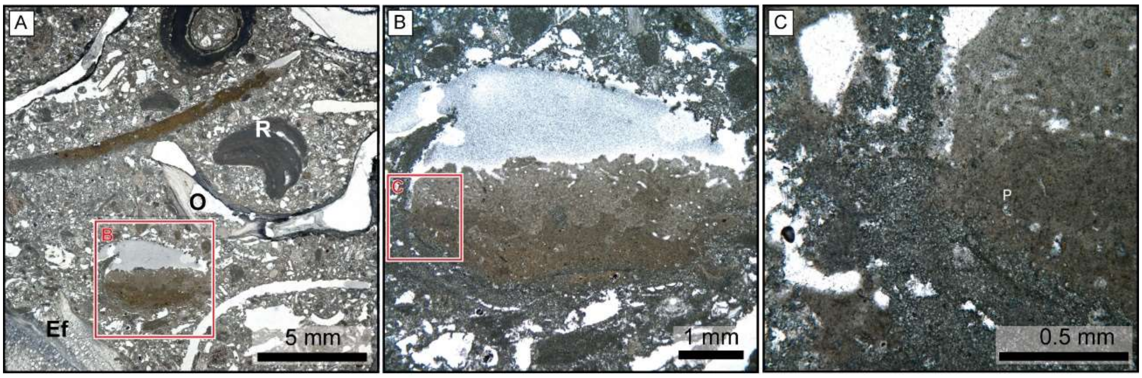

Figure 8

Figure 8: Microphotograph of the geopetal infill in the foralgal floatstone at Site U1465 (69.15 mbsf) modified from Betzler et al. (2017). (A.) Foralgal floatstone facies with abundant mollusk molds, some with geopetal infill (red frame), red algae (R), encrusting foraminifera (Ef), and partially dissolve oyster fragments (O). (B) Close-up of the geopetal infill in a mold (red frame indicates the position of C). Two different generations of geopetal infill have different brown shades. The uppermost part of the infill displays evidence of bioerosion. (C) Close-up of the contact between the host rock and the geopetal infill with a small planktonic foraminifer (P) floating in the micritic matrix.

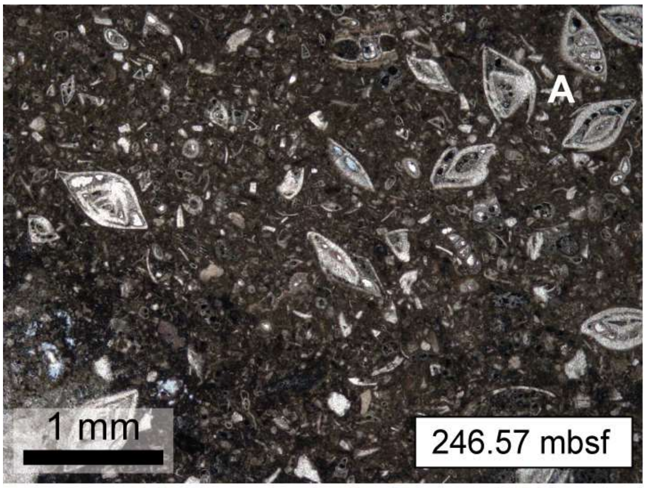

Figure 9

Figure 9: Microphotograph of a mixed benthic foraminifera packstone with abundant *Amphistegina* (A).

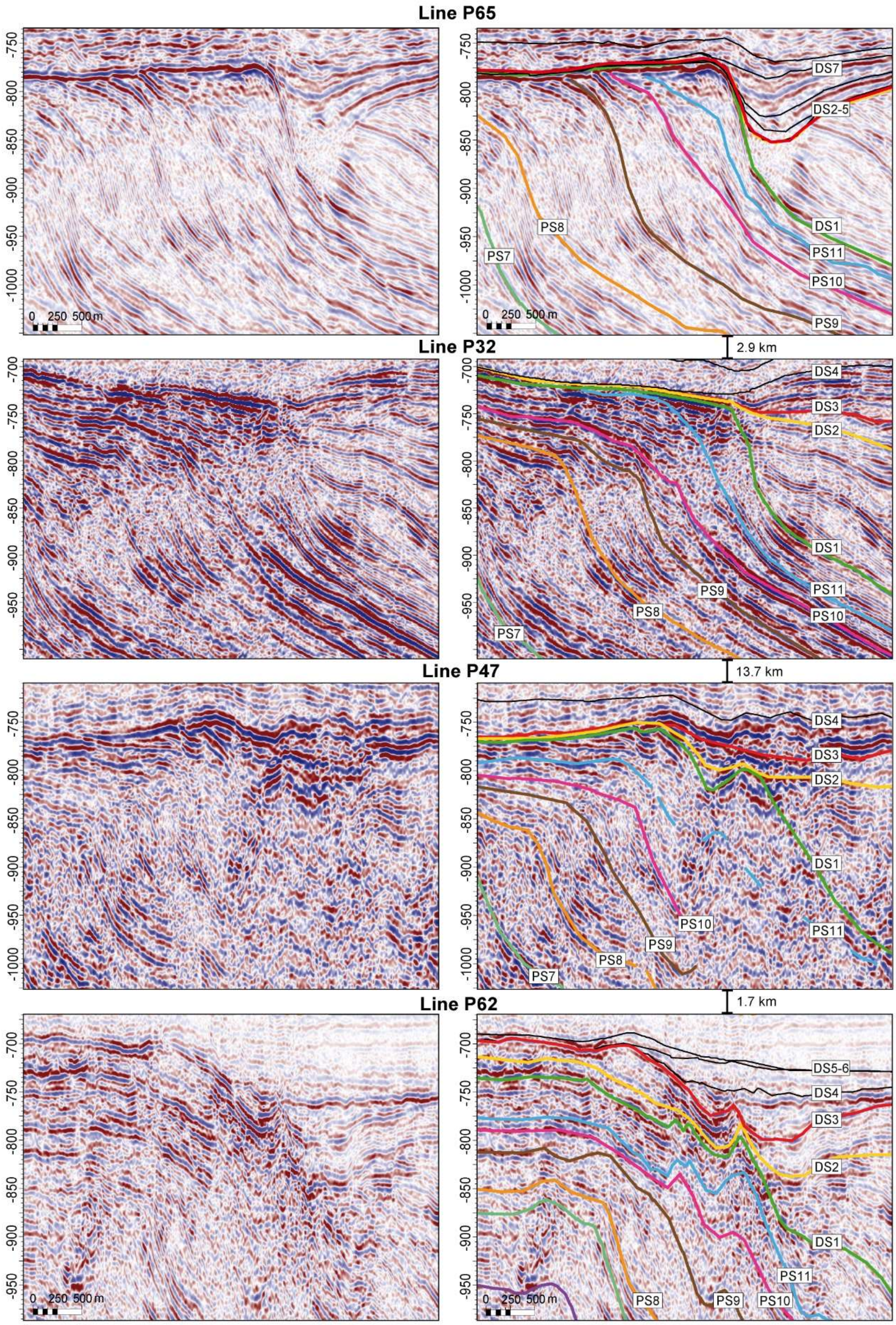

Figure 10

Figure 10: Close view of seismic Line P65 and line drawing. Stratigraphic column of Site U1465. Left axis and right axis present the two-way travel time TWT [ms].

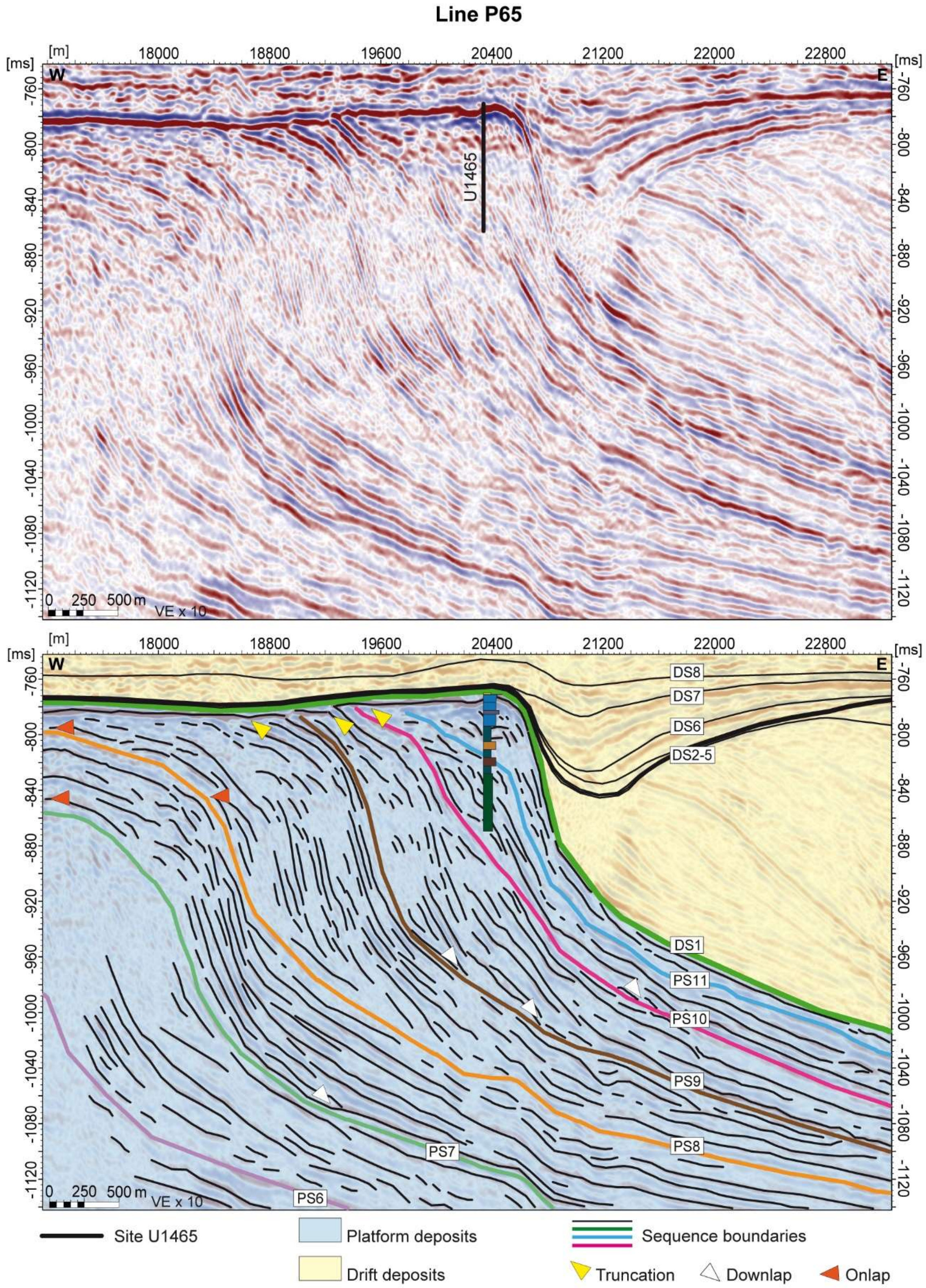

Figure 11

Figure 11: Uninterpreted (left) and interpreted (right) segments of seismic lines across a margin of a drowned carbonate bank. For the location of the lines see Fig 1. All lines have

same WE orientation, same scale 1:35000 and same vertical exaggeration VE x 10. The left axis presents the two-way travel time TWT [ms].

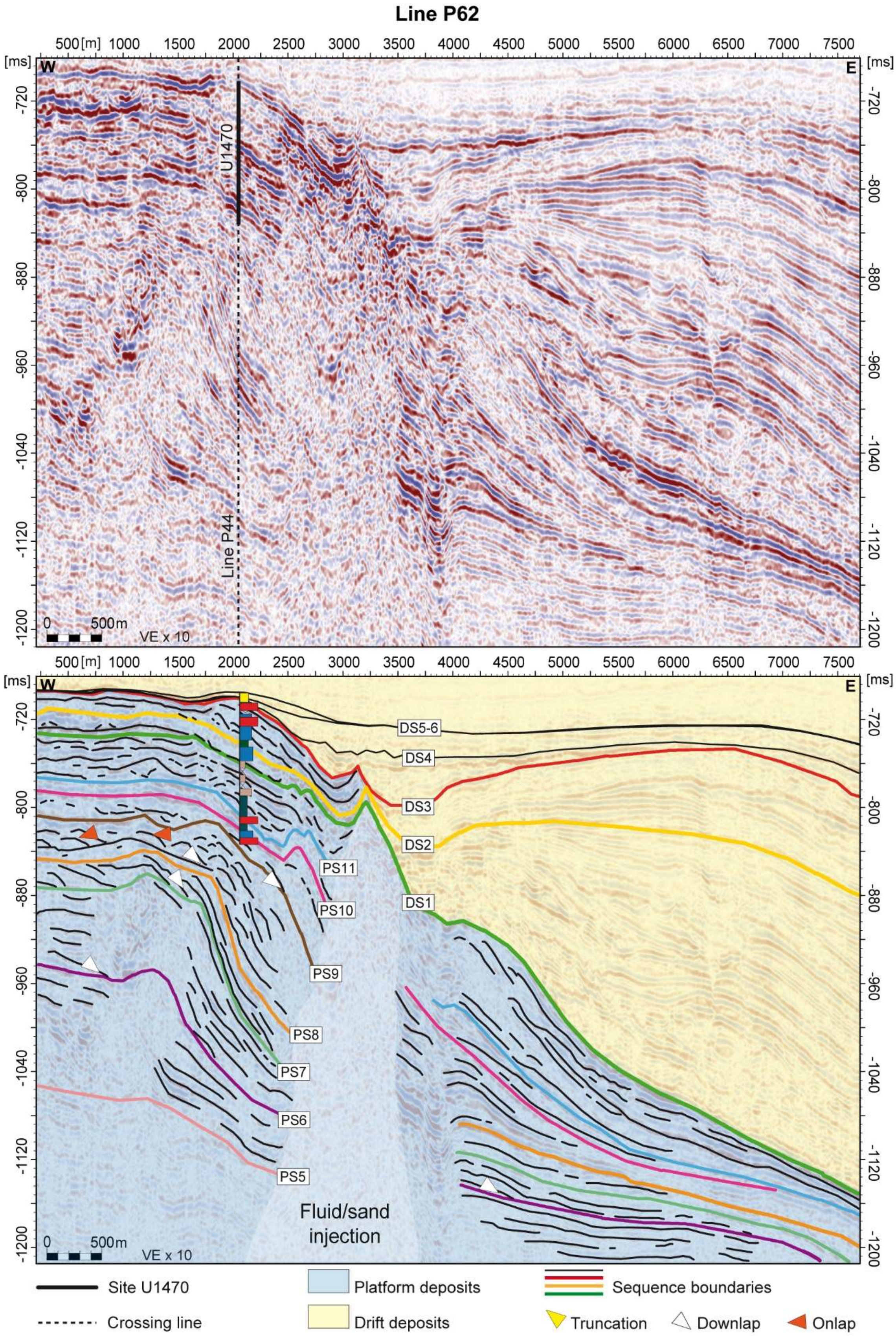

Figure 12

Figure 12: Close view of seismic Line P62 and line drawing. Stratigraphic column of

Site U1470. Part of the geometries in this line is masked by the injection of fluids or sand in the slope area. Left axis and right axis present the two-way travel time TWT [ms].

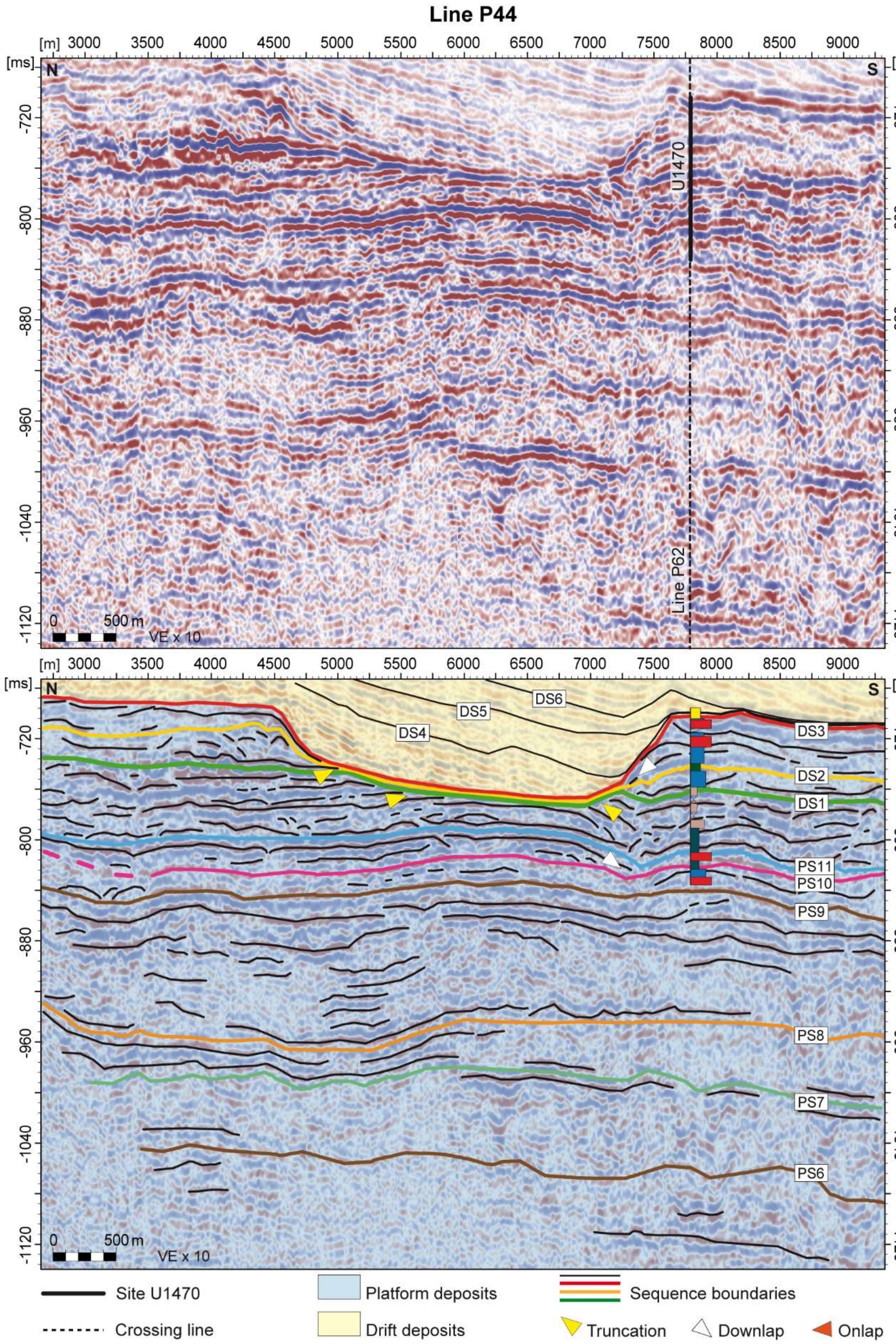

Figure 13

Figure 13: Closer view of seismic Line P44, perpendicular to line P62, and line drawing.

Stratigraphic column of Site U1470. Left axis and right axis present the two-way travel time TWT [ms].

Name	Texture	Components	Coatings	Occurrence	Position
Coral-coralline algal boundstone	Mostly boundstone texture. The sediment trapped in the pockets among the corals is a wackestone to packstone.	Abundant coral and red algae (up to 44%). Red algae occur as nodules and crust over corals. Common to few silt-sized unidentifiable bioclasts. Rare *Halimeda* and LBF (*Amphistegina*, and sparse *Operculina*, *Borelis* and *Marginopora*), mollusks, echinoids, and benthic and planktonic foraminifera. Intraclasts may be present.	Red algae (*Adeylithon* and *Neogoniolithon*), encrusting foraminífera (*Acervulina* and *Homotrema*), and bryozoan.	The matrix is micritic locally very sparse. *Gastrochaenolites* is the only sediment structure observed. Porosity varies between 15-25% and comprises of moldic and intraskeletal pores.	U1465: PS11. U1470: PS9, PS10 and DS2.
Foralgal floatstone-rudstone	There is a N-S variation with rudstone-grainstone dominated facies at Site U1465 and floatstone-packstone dominated facies at Site U1470.	LBF are common (up to 24%). The dominant genus is *Amphistegina*, followed by *Operculina*, *Borelis*, *Marginopora, Miogypsina*, *Lepidocyclina*, *Nummulites*, *Alveolina*, and *Sorites* are also present. Red algae are common as up to 2 cm-nodules and fragments. Up to 5-cm mollusk fragments (including oysters) are	Red algae (*Neogoniolithon and Adeylithon, Lithothamnion, Lithophyllum, Harveylithon, Hydrolithon, Mesophyllum, and unidentifiable Melobesiod*), encrusting foraminífera, and bryozoans. Locally serpulids are present.	The bioclasts are floating in a micrite matrix (more abundant at Site U170). *Gastrochaenolites* is documented. At U1465, mollusk molds and partially dissolved red-algal nodules present geopetal structures that consist of fine mud supporting micron-sized bioclasts and planktic foraminifera fragments. The intraclasts at Site U1465 are rounded and contain silt-sized unidentifiable bioclasts, immersed in a fine, dark-micrite matrix.	U1465and U1469: PS11. U1470: PS9, DS1 and DS2.

		common and *Halimeda* are few through the facies. Benthic foraminifera (mostly miliolids) are rare. Unidentifiable bioclasts, echinoids spines and plates, corals, planktic and encrusting foraminifera, bryozoans, serpulids and intraclasts are present.		Intraclasts at Site U1470 present benthic foraminifera and larger unidentifiable bioclasts in a recrystallized-micrite matrix. The porosity varies between 15-25% and it comprises largely moldic pores and to a lesser extent intraparticle pores.	
Rhodalgal rudstone	Rudstone.	Red algae are widely present as nodules and fragments (up to 40%). *Halimeda* and unidentifiable bioclasts are common. Small benthic foraminifera are rare and two thirds of them are miliolids. Large benthic foraminifera are rare and represented by *Amphistegina* and fragments of *Operculina*. Other components are mollusks molds, echinoids, corals and encrusting foraminifera.	Red algae (*Adeylithon*) and encrusting foraminífera (*Homotrema*).	The matrix consists of micrite and recrystallized micrite. No sedimentary structures were found. Rare, dark-brown to black oxides accumulations occur. Porosity is 10-15% and comprises moldic and intraskeletal porosity.	U1465: PS11.
LBF grainstone	Mostly grainstone to mud-lean packstone, locally rudstone where the LBF are	Abundant LBF (up to 36%) including *Amphistegina*, *Cycloclypeus*, and *Operculina*. *Miogypsina*, *Lepidocyclina*, *Marginopora*, *Borelis*, *Sorites*, *Nummulites*, and *Alveolinella* also occur.	Encrusting foraminífera (*Homotrema*), bryozoan, and red algae (*Adeylithon, Sporolithon, Lithophyllum*, *Harveylithon*, *Lithoporella*, *Porolithon*, *Neogonilithon*,	Matrix is scarce and mostly microgranular. No sedimentary structures were found in this facies. The intraclasts have a distinct, usually darker colored matrix, which supports micron-	U1465: PS10. U1470: DS1.

	especially abundant.	*Halimeda* plates vary from present to abundant. There are few to common benthic foraminifera and a third of the total amount corresponds to miliolids. Apart from miliolids small benthic foraminifera with porcelaneous and agglutinated tests were observed. Unidentifiable bioclasts are common. Red algae are few and occur mostly as fragments. Echinoids spines and plates are rare to few and pieces up to 7 mm were found. Mollusks and planktic foraminifera are rare.	and *Hydrolithon*).	sized unidentifiable bioclasts or locally fragments of planktic and benthic foraminifera. The intraclasts are mostly rounded, rarely sub-angular and were found in various sizes Porosity was estimated to 10-25%.	
LBF floatstone-packstone	Floatstone to packstone. Usually a packstone with some large components.	Large benthic foraminifera are common in this facies (up to 25%) represented by *Operculina*, *Amphistegina*, and *Cycloclypeus*. *Borelis* and *Lepidocyclina* are also present. Benthic as well as planktic foraminifera are relatively rare. Up to 2 cm coral debris are rare to few. Red algae are present exclusively as fragments. In minor amounts there are	Encrusting foraminífera (*Acervulina*), bryozoan, and red algae (*Neogoniolithon*, *Lithothamnion*, *Harveylithon*, and *Adeylithon*).	The bioclasts are embedded in a dense micrite matrix. No sedimentary structures were observed in this facies. The porosity varies between 15% to 20% and mostly consists of moldic pores.	<u>U1465:</u> PS11.

		unidentifiable bioclasts, *Halimeda*, mollusks molds and fragments, and echinoids.			
LBF packstone to grainstone	Packstone to grainstone (commonly mud-lean packstone).	LBF are abundant (up to 29%) with *Amphistegina* followed by *Cycloclypeus* and *Operculina* in similar proportion, and *Lepidocyclina*, *Borelis*, *Nummulites*, and *Miogypsina* in smaller amounts. *Halimeda* plates are common. Red algae are present as fragments, nodules, and minor as encruster. Smaller benthic foraminifera are rare to few, and a quarter of the total amount is represented by miliolids. Planktic foraminifera are rare to few and occur in the entire facies. Unidentifiable bioclasts, echinoids, mollusks molds and fragments, corals, encrusting foraminifera, and bryozoan are also present.	Red algae (*Adeylithon* and *Neogoniolithon*), encrusting foraminífera, and bryozoans.	The components are embedded in a micrite-poor matrix. No sedimentary structures were observed in this facies. Red algae nodules present borings. The porosity varies between 20-25% and it comprises mainly moldic pores and minor intraskeletal pores.	<u>U1465:</u> PS10 and PS11. <u>U1470:</u> PS10 and PS11.
LBF-rudstone	Rudstone.	Large benthic foraminifera are abundant (up to 53%) dominated by *Amphistegina* with fewer *Operculina*, *Cycloclypeus*, and *Lepidocyclina*.	Red algae (*Adeylithon* and *Neogoniolithon*) and bryozoan.	The matrix is poor and consists of micrite. No sedimentary structures were observed except for a *Gastrochaenolites*. Porosity is 15-20% and includes	<u>U1465:</u> PS10.

		Planktic foraminifera are rare to few. Benthic foraminifera are rare. Unidentifiable bioclasts, mollusks, echinoids, and *Halimeda* are present.		moldic and intraparticle-pores.	
Mixed benthic foraminífera packstone to floatstone.	The texture varies from packstone to a floatstone. Usually a packstone with some large components.	Large benthic foraminifera are abundant (up to 29%) with *Amphistegina* and *Miogypsina* being the predominant genera, and *Marginopora*, *Operculina*, *Borelis*, *Sorites*, and *Lepidocyclina* in smaller proportion. Smaller benthic foraminifera are common (mostly miolids but also uniserial, biserial, trochospiral, planspiral forms). Mollusks are also common including large oyster pieces were found. Other components are unidentifiable bioclasts, echinoids, *Halimeda*, bryozoans, planktic foraminifera, red algae, and intraclasts. Scarce planktic foraminifera may occur.	Bryozoan and red algae (*Adeylithon* fragments).	The matrix consists of dense micrite, locally recrystallized. No sedimentary structures were observed. The average porosity is 15% and includes moldic and intraparticle pores.	U1470: PS11.

Table 1: Summary of the main facies recorded at IODP Exp. 359 Sites U1465, U1469, and U1470.